Sustainable Energy & Fuels

Dynamic Study of Direct CO2 Capture from Indoor Air using Poly(ethylenimine)-Impregnated Fiber Sorbents

Journal:	*Sustainable Energy & Fuels*
Manuscript ID	SE-ART-05-2023-000618.R1
Article Type:	Paper
Date Submitted by the Author:	17-Jul-2023
Complete List of Authors:	Kong, Fanhe; Georgia Institute of Technology, Chemical and Biomolecular Engineering Rim, Guanhe; Georgia Institute of Technology, Chemical and Biomolecular Engineering Priyadarshini, Pranjali; Georgia Institute of Technology, Chemical and Biomolecular Engineering Song, MinGyu; Georgia Institute of Technology, Chemical and Biomolecular Engineering Realff, Matthew; Georgia Institute of Technology, Chemical & Biomolecular Engineering Lively, Ryan; Georgia Institute of Technology, School of Chemical & Biomolecular Engineering Jones, Christopher; Georgia Institute of Technology, Chemical and Biomolecular Engineering

Dynamic Study of Direct CO_2 Capture from Indoor Air using Poly(ethylenimine)-Impregnated Fiber Sorbents

Fanhe Kong, Guanhe Rim, Pranjali Priyadarshini, MinGyu Song, Matthew J. Realff, Ryan P. Lively,* Christopher W. Jones*

School of Chemical & Biomolecular Engineering, Georgia Institute of Technology, Atlanta, GA 30332

Emails: ryan.lively@chbe.gatech.edu, cjones@chbe.gatech.edu

Abstract

Supported amine adsorbents are promising materials for direct air capture (DAC) of CO_2 due to their high CO_2 capacity and relatively low energy requirement for regeneration. For a DAC process, it is essential to properly define operating parameters to achieve high sorbent productivity (amount of CO_2 captured per unit quantity of sorbent material over unit time). It is furthermore essential to understand the kinetic behavior of the process under the influence of various operating conditions such as the inlet air velocity, sorbent composition, and humidity to select an effective range of operating conditions to maximize sorbent productivity. Here, the dynamic behavior of a DAC process is probed using a fixed fiber sorbent contactor containing poly(ethylenimine) (PEI)-impregnated composite silica/cellulose acetate (CA) fibers. Experiments are conducted using both simulated air (398 ppm CO_2 balanced by N_2) and real indoor air (~400-500 ppm CO_2). The experimental behavior of the fibers using simulated air and indoor air is compared, and the influence of the inlet air velocity on the breakthrough behavior is assessed. By changing operating conditions, the impact on the fiber sorbent productivity (mmol CO_2 ▪ g_{fiber}^{-1} ▪ h^{-1}) is quantified to identify conditions that could favor high rates of CO_2 removal. The kinetics of steam-assisted CO_2 desorption are studied, identifying achievable desorption times. Productivities of 1.2 mmol CO_2 ▪ g_{fiber}^{-1} ▪ h^{-1} are obtained using an inlet air velocity of 1.1 m/s. Performance trends show that further increasing the inlet air velocity will likely lead to even higher productivities.

1. Introduction

To effectively halt and reverse climate change, it is essential to develop methods that can directly remove CO_2 from the atmosphere, producing "negative emissions," to achieve a net reduction in the atmospheric CO_2 concentration. Two classes of technologies exist that can lead to a net reduction in the atmospheric CO_2 concentration. The first is chemistry-based direct air capture technologies (DAC),[1–8] and the second is bio-based systems such as bioenergy with carbon capture and storage technologies (BECCS).[9,10] The advantages of DAC over BECCS include less land use per unit amount of CO_2 captured[11–14] and potential to be deployed around the globe,[15] including places unsuitable for plant growth or harvesting. The advantages of BECSS over DAC include the creation of a valuable co-product (energy). For DAC, multiple approaches have been proposed and studied, as summarized in the review papers by Sanz-Perez et al.[16] and Zhu et al.[17] Among the proposed DAC technologies,[18–27] amines supported on solid substrates have been shown to be particularly promising,[28–33] and a variety of amine molecules[34–38] and support materials[39–42] have been studied. Recently, additional research efforts have been devoted to DAC at cold temperatures to promote the application of DAC across a wider geographical expanse.[15,42–44]

In practical DAC units, it is essential to ensure a low pressure drop in the DAC unit to reduce the energy consumption in moving the ambient air and reduce the associated operating costs.[45–51] Therefore, it is crucial to select an appropriate contactor configuration that can lead to a minimal pressure drop. Sorbents in the shape of monoliths and fibers have been studied in the past and both are proven to be promising contactor structures with low pressure drops and relatively fast mass transfer.[52–57] This study focuses on amine-impregnated fiber materials for DAC applications.[53,58]

In the past, a large number of studies have been conducted on fiber sorbents for CO_2 separation from flue gas.[59–64] Recently, research efforts have shifted toward using these materials for DAC applications. Sujan et al.[53] studied the use of poly(ethylenimine) (PEI)-loaded silica fibers for CO_2 capture from simulated air and reached pseudoequilibrium CO_2 capacities of 0.59 and 1.6 mmol CO_2/g fiber from breakthrough experiments under dry and humid conditions, respectively. Wilfong et al.[54] studied directly spun epoxy-crosslinked PEI fiber sorbents and reached a CO_2 capacity of 0.2 mmol CO_2/g fiber during DAC cycling experiments in a ten-fiber module. Armstrong et al.[65] studied the system kinetics of DAC by sorbent-containing porous electro-spun fibers made with the solvothermal polymer additive removal technique, reaching a high cyclic capacity with an estimated productivity of 1.4 mmol CO_2 per gram-hour. Sekizkardes et al.[66] investigated fibers of

polymers of intrinsic microporosity (PIM) based on amidoxime and amine functionalities for DAC, and achieved a 0.8 mmol CO_2/g fiber uptake and a rapid CO_2 adsorption rate (5 minute adsorption cycle). Zhang et al.[67] studied tetraethylenepentamine-grafted polyacrylonitrile (TEPA@PAN) hollow fibers and achieved a CO_2 capacity of 2.03 mmol/g at ambient CO_2 concentration. Despite these above studies, to date, there is a dearth of research data published on CO_2 adsorption kinetics using real ambient air in a system setup mimicking realistic industrial DAC, especially on fibrous materials. Most kinetics studies have instead been focused on post-combustion CO_2 capture.[68,69] For the scale-up and commercialization of DAC technologies using fiber sorbents, it is essential to understand the fiber performance in ambient air, which may differ from simulated air due to the presence of varying humidity and several trace components. In addition, in industrial-scale DAC operations, air velocities as high as several meters per second may be applied to ensure rapid loading of the adsorbent. In contrast, breakthrough studies conducted so far in the laboratory have only reached air velocities on the magnitude of ~0.1 m/s.[53] Thus, there is a knowledge gap between the operating conditions of lab-scale tests and what is needed for commercial-scale applications of fiber sorbents.

The objective of this work is to analyze the dynamic performance of fiber sorbents using ambient indoor air. CO_2 breakthrough tests were conducted using both simulated air and real indoor air and the results are compared. The influence of operating conditions such as inlet air flowrates and PEI loadings on the system's dynamic performance is analyzed. The operating conditions leading to maximum CO_2 productivity are identified. Moreover, the desorption phase was also studied via indirect contact steam heating as a preliminary verification of reasonably fast desorption kinetics.

2. Materials and Methods

2.1. Materials

Cellulose acetate (CA) (MW 50,000 Da) was purchased from Sigma-Aldrich Inc. Amorphous silica (C-803) was purchased from Grace Davison Inc. N-Methyl-2-pyrrolidone (NMP) (Reagent Plus, 99%) was purchased from Sigma-Aldrich and used as the solvent for polymer-dope preparation. Poly(vinylpyrrolidone) (PVP) (MW 55,000 Da) was purchased from Sigma-Aldrich and used as the pore-forming agent for the open-pore network in the polymer/silica fiber sorbents. Methanol (ACS Grade) and *n*-hexane (ACS Grade) were purchased from VWR. They were used in the solvent-exchange step to remove water and residual NMP in spun fibers. All solvents were used as received from the manufacturer with no purification or modification. Branched PEI (MW 800

Da) was purchased from Sigma-Aldrich and used as the amine source in post-spinning functionalization. Single-component gases and gas mixtures were purchased from Airgas as ultrahigh-purity (UHP) grade. A gas mixture of 398 ppm of CO_2/balance N_2 i.e. simulated air, was used for breakthrough experiments.

2.2. Preparation of Fiber Sorbents

CA-silica fibers were spun via the dry-jet, wet quench spinning technique using a custom-built fiber spinning line. The silica/CA ratio used for making the polymer dope was 60:40 wt%, which is close to the practical maximum. All polymers and silica were dried under 25 in Hg vacuum at 110 °C for 12 hours before being made into the polymer dope. More technical details on the silica fibers and the spinning procedure can be found in previous literatures.[53,58,64]

After spinning, the fibers were impregnated with PEI via the following impregnation procedure: fibers were soaked in a vial containing 50 mL methanol. Then, PEI was added to the vial until reaching the desired concentration. Three types of fibers were prepared in separate vials with different PEI concentrations (10 wt%, 15 wt%, and 20 wt%). The amount of fiber in each vial was approximately 3 g. The vials were placed horizontally during the impregnation. The fibers stayed in the PEI solutions for 4 hours at 20 °C. Then, the impregnated fibers were solvent-exchanged with *n*-hexane. Finally, the impregnated fibers were dried at ambient temperature and pressure overnight.

2.3. Fiber Characterization

Scanning electron microscopy (SEM)

SEM was performed on a Hitachi SU8230 with a cold field emission gun at an accelerating voltage of 3 kV and an emission current of 10 μA.

N_2 physisorption

N_2 physisorption was conducted for pristine and impregnated fibers at 77 K on a surface area and porosity (SAP) system (autosorb iQ/Quantachrome). In each experiment, ~100 mg of fiber sample was activated at 110 °C for 6 h before the measurement. The BET surface area was estimated using the N_2 physisorption data in the P/P_0 range of 0.05 to 0.2.

CO_2 adsorption

The equilibrium CO_2 adsorption performance of PEI-CA-SiO_2 fibers was measured at 25 °C using an SAP system (autosorb iQ/Quantachrome). In each experiment, ~100 mg of fiber sample was

activated at 110 °C for 6 h before the measurement. An equilibration interval of 1 min was used, where the cell pressure was checked every 1 min and compared until the pressure in the cell was within the pressure tolerance (manufacturer tolerance setting 0). If the cell pressure dropped below the lower limit of the P/P_0 tolerance, the data point was stored.

TGA combustion experiments

The compositions of the pristine and impregnated fibers were estimated by TGA combustion experiments. The TGA equipment was a Q500 from TA instrument. In the experiment, the temperature was first increased from room temperature to 200 °C at 10 °C / min and kept at 200 °C for 1 hour under N_2 to remove all adsorbed CO_2 and H_2O. Then, the temperature was increased to 900 °C by 10 °C / min under simulated air (79% N_2 and 21% O_2, different from the simulated air mentioned elsewhere in this paper, which did not contain O_2) to burn off all organic components. The weight loss between 200 and 900 °C was the weight of organic component, i.e., CA and PEI, while the remaining weight at the end of the experiment was the weight of silica. From the results, the CA/silica weight ratio of the pristine fibers, as well as the PEI loading of impregnated fibers, were calculated.

2.4. Experimental System Setup

The system for the breakthrough experiments consisted of a simulated air injection system, an ambient air injection system, and a steam delivery system, as shown in **Figure 1**. In the ambient air injection system, three fans were placed in series to provide the required pressure to drive the air through the sorbent module. In this work, the maximum air velocity achieved by using three fans was 1.1 m/s.

A speed controller was installed to allow the fans to operate at lower power to provide lower air velocities when needed. This allowed the fans to provide an inlet air velocity as low as 0.17 m/s, a condition also tested in this work. The ambient air was propelled by the fans to flow through a flowmeter before entering the sample module to measure the air flowrate. The outlet gas was connected to a LI-850-3 LI-COR detector purchased from LI-COR Biosciences to measure the CO_2 and H_2O concentrations. Right before and after each adsorption test, the CO_2 concentrations in air were measured and the average of the two values was used in calculating the CO_2 uptake for that adsorption test. For all tests using indoor air conducted in this work, the CO_2 concentration in air was between 400 and 500 ppm.

The fiber module was a 20-cm long stainless-steel tube with an inner diameter of 0.43 cm. Inside, 40 PEI-CA-SiO_2 fibers filled the fiber module. The void fraction in the module was 63%.

Before the adsorption experiment, the fiber module was wrapped with a heating tape, which heated the fibers to 110 °C under flowing N_2 for 30 min to remove the adsorbed CO_2 and H_2O. Then, the heat was turned off and the fibers were allowed to cool down to room temperature (~25 °C) with the same N_2 flow. For the tests using simulated air, 398 ppm CO_2 balanced by N_2 was passed through the fixed bed; for the tests using ambient air, indoor air was propelled by the fans to pass through the fixed bed. For the tests using ambient air, the inlet ambient CO_2 concentration was measured right before and after each adsorption test, and the average of the two values was used as the ambient CO_2 concentration for that adsorption test. Both the inlet and outlet gas CO_2 and H_2O concentrations were measured by the LI-COR detector.

After the adsorption phase, the fibers were regenerated under N_2 flow at 110 °C for 10 min, and the modules were cooled following the same protocol before the next adsorption-desorption cycle.

For experiments involving humidity, a pre-humidification step was added after the post-desorption cooldown and before the next adsorption phase. N_2 was passed through a bubbler containing a saturated salt solution of KCl in deionized water before entering the fixed bed. The saturated KCl solution set the outlet gas RH at 85%. The vapor concentration of the outlet gas was monitored by the LI-COR detector to ensure that the fibers were fully saturated with H_2O before starting the adsorption. After reaching complete hydration of the sample, the inlet gas was switched to simulated air of 85% relative humidity (RH) reached by passing the gas through another bubbler containing KCl solution.

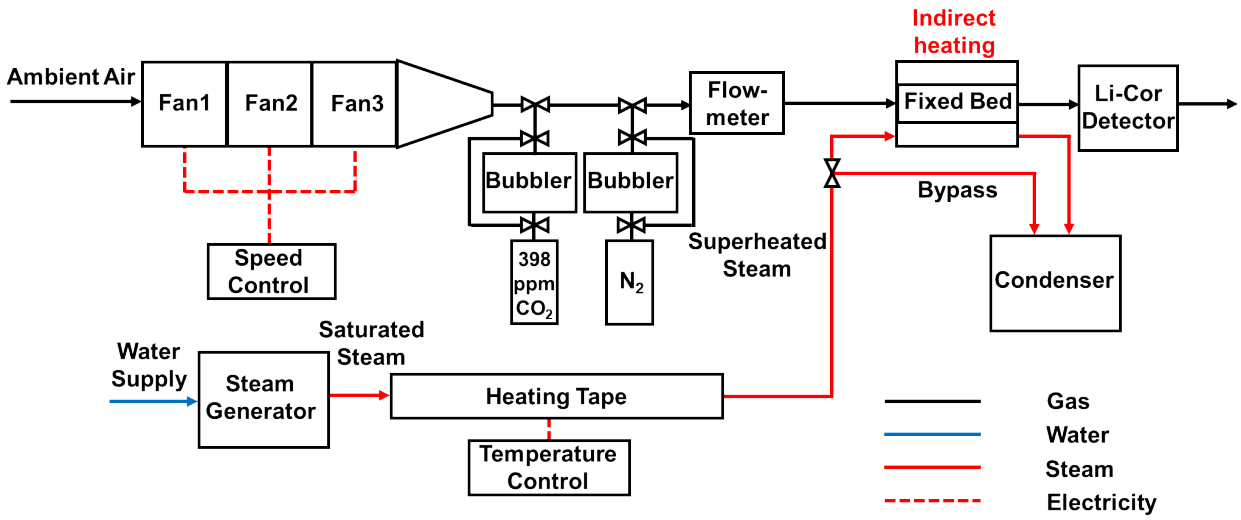

***Figure 1**. Schematic diagram of the experimental system used to perform both adsorption and desorption experiments. The system consists of a simulated air injection system, an ambient air injection system, and a steam delivery system for desorption by indirect heating.*

The steam delivery system is also depicted in **Figure 1**. Water was converted into saturated steam in the steam generator. The saturated steam then flowed through a tube wrapped with heating tape to be further heated. The superheated steam then entered the heating jacket surrounding the fixed bed where the fiber sample was placed. The superheated steam exchanged heat with the sample via indirect contact heating. Finally, steam was condensed into water in the condenser.

The steam generation rate of the steam generator was 5.8 g/min. The temperature of the heating tape was set at 130 °C. Calculations showed that this provides a thermal input of 5.8 W into the sample module if only the sensible heat of the steam is used, and 224 W if the latent heat of condensation is also used.

During the test, the steam generator and the heating tape were turned on for at least one hour for thermal stabilization before starting the experiment. During this period, the steam generated flowed through the bypass line to directly reach the condenser. After achieving a stable steam flow, 500 sccm N_2 was flowed into the fixed bed to sweep out the O_2 from the bed, where fibers with CO_2 sorbed to pseudo-equilibrium conditions were present. Next, steam entered the heating jacket surrounding the fixed bed. This point was recorded as the starting point of the desorption phase. The outlet gas composition was measured by the LI-COR detector. The reason for re-

diluting the adsorbed CO_2 with N_2 was that the LI-COR detector could not accurately measure CO_2 concentrations above 2%, and hence a sufficiently high N_2 flow through the fixed bed was needed for the peak concentration of CO_2 in the outlet gas to be less than 2%. This allowed accurate measurements of the amount of CO_2 desorbed as well as the CO_2 desorption kinetics. This desorption study was more focused on CO_2 desorption kinetics, and the CO_2 purity of the desorbed gas would be the objective of future studies.

3. Results and Discussion

3.1. Characterization of Amine-Functionalized Sorbents

SEM images were taken of the as-spun fibers, as shown in **Figure 2**. The fibers have an average diameter of 410 microns. SiO_2 particles with an average size from 3 to 6 μm appear to be held in place by the surrounding polymer matrix and are uniformly embedded throughout the polymer matrix. No observable skin layer was noted on the outside of the fiber.

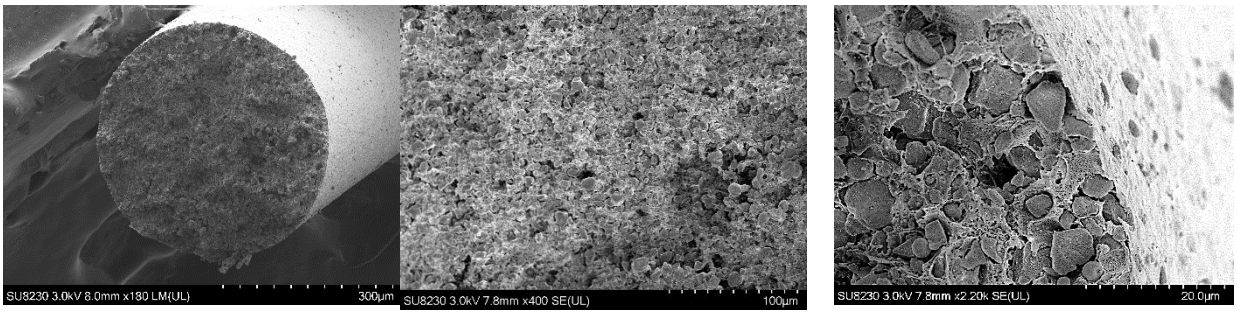

Figure 2*. SEM images of as-spun fibers. (a) the entire cross-section of a fiber. (b) the cross-section of a fiber further magnified. (c) the cross-section of a fiber further magnified to show the SiO_2 particles held by the surrounding polymer matrix and the outer surface of the fiber sorbent.*

The composition of pristine fibers was estimated by TGA combustion experiments.

The silica to CA weight ratio was calculated using Equation 1:

$$\frac{m_{silica}}{m_{CA}} = \frac{\text{sample wt after combustion}}{\text{initial sample wt} - \text{adsorbed } CO_2, H_2O \text{ wt} - \text{sample wt after combustion}} \quad (1)$$

The silica weight fraction of the pristine fibers was calculated to be 52%, which was slightly lower than the weight fraction in the dope (60%), indicating some silica loss during the fiber spinning. This observation is consistent with a previous study.[53]

The PEI loading in the CA-SiO_2 fibers was also estimated by TGA combustion experiments. The PEI loading was quantified as grams of PEI per gram of silica in the fiber, as calculated using the Equation 2, where the weight of CA could be calculated using the silica/CA weight ratio calculated in the previous step:

$$\frac{m_{PEI}}{m_{silica}} = \frac{\text{initial sample wt} - \text{adsorbed } CO_2, H_2O \text{ wt} - \text{sample wt after combustion} - \text{CA wt}}{\text{sample wt after combustion}} \quad (2)$$

The fibers impregnated with three different PEI concentrations were also combusted in the TGA to assess their PEI loadings, and the results are shown in **Figure 3**. As shown in the figure, the PEI loading increases with an increasing PEI concentration in the impregnation solution. The PEI loadings obtained using 10, 15 and 20% PEI solutions are 0.37, 0.68, and 1.04 g PEI/g SiO_2, respectively. These three fibers are denoted as 0.37PEI@SiO_2, 0.68PEI@SiO_2, and 1.04PEI@SiO_2, respectively. Compared to a previous study,[53] the PEI loadings obtained in this work are lower when using the same PEI solution concentration. With a 10% PEI solution, the PEI loading in this work is 0.37 g PEI/g SiO_2, as compared to 0.7 g PEI/g SiO_2 in the previous work. In the previous work it was found that fibers impregnated in PEI concentrations above 10% became gel-like, with a noticeable degree of swelling, and could not be practically assembled into fiber modules. In this work, however, fibers impregnated in the 20% PEI solution still retained their physical integrity and could be assembled into sample modules. This difference suggests that the fibers used for this study might be more compact and less porous than those used previously, and the cause for such a difference is attributed to some nuanced differences in the spinning procedure.

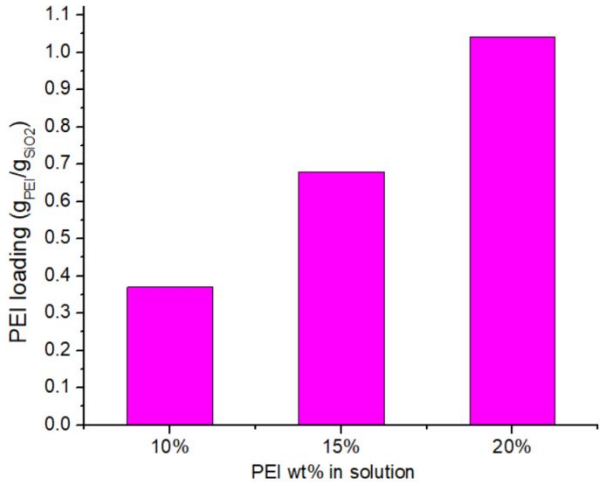

***Figure 3**. PEI loading on the fibers with different PEI wt% in methanol during impregnation. Impregnation was performed at 20 °C for 4 h, with sample containers placed horizontally.*

N_2 physisorption was conducted on pristine and impregnated fibers, and the results are shown in **Figure 4**. The results indicate that the amount of physisorbed N_2 decreases with an increasing PEI loading. The surface area and pore volume of each fiber sample were calculated and are shown in **Table 1**. With an increasing PEI loading, the surface area and pore volume decrease rapidly, suggesting that PEI has been successfully impregnated into the fibers. Compared to the previous study,[53] the pristine fibers in this study show higher surface areas but lower total pore volumes. Additionally, the surface areas and pore volumes after impregnation are much higher than those in the previous work using the same PEI concentration. This difference is likely due to nuanced differences in the spinning procedures, as both studies used the same batch of silica. This likely also caused the lower PEI loading seen in this work using the same PEI concentration for impregnation.

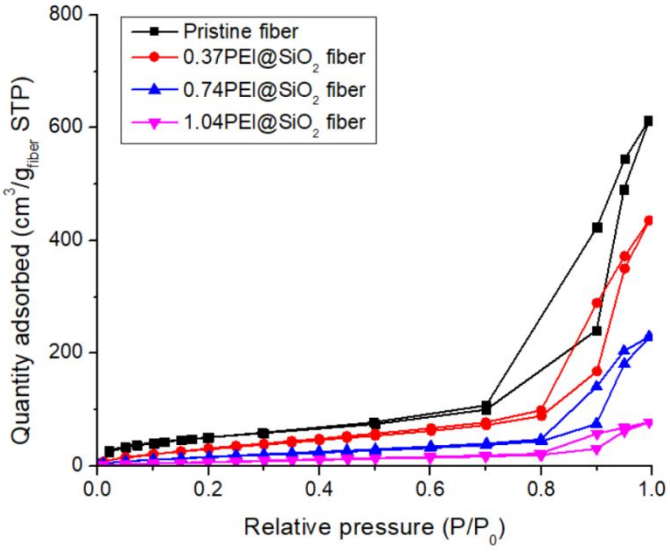

***Figure 4**. N_2 physisorption curves of pristine and impregnated fibers.*

***Table 1**. BET surface areas and pore volumes of pristine and impregnated fibers*

Sample	BET (m^2/g fiber)	Pore vol. (cm^3/g fiber)
Pristine	183	0.76
0.37PEI@SiO_2	133	0.54
0.74PEI@SiO_2	68	0.28
1.04PEI@SiO_2	31	0.10

CO_2 isotherms of pristine fibers, 0.37PEI@SiO_2 fibers, and 1.04PEI@SiO_2 fibers are shown in **Figure 5.** The impregnated fibers show much higher CO_2 uptakes than pristine fibers, and the 1.04PEI@SiO_2 fibers show higher CO_2 uptakes than 0.37PEI@SiO_2 fibers. Moreover, the advantage in CO_2 uptake of the impregnated fibers over pristine fibers, and the advantage in CO_2 uptake of the 1.04PEI@SiO_2 fibers over 0.37PEI@SiO_2 fibers, are more pronounced at lower pressures.

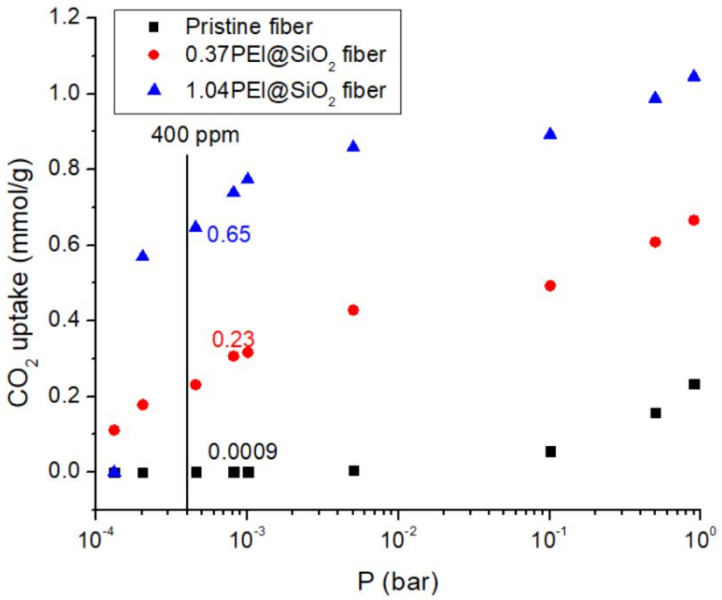

***Figure 5**. CO_2 uptakes of pristine and impregnated fibers measured in the SAP instrument @ 25 °C with ~100 mg of fiber sample. Activation @ 110 °C for 6 h. Equilibration interval = 1 min. The CO_2 uptakes are 0.0009, 0.23, and 0.65 mmol/g on pristine fibers, 0.37PEI@SiO_2 fibers, and 1.04PEI@SiO_2 fibers, respectively.*

3.2. Comparison between Ambient and Simulated Air

Following the dry isotherm measurements, we explored CO_2 sorption using simulated and real indoor air. During the experiments, the ambient indoor air contained 45 ± 5% relative humidity (RH). This could lead to an increase in CO_2 uptake compared to dry simulated air cases, as moisture assists CO_2 uptake by supported amine sorbents.[53] This influence of humidity on the system performance was studied by comparing the CO_2 uptakes using indoor air and simulated air. The 1.04PEI@SiO_2 fibers were used for this set of experiments. Three breakthrough tests were conducted at an inlet air velocity of 0.57 m/s, using (i) dry simulated air, (ii) indoor air with 45 ± 5% RH, and (iii) simulated air with 85% RH achieved by passing it through a saturated KCl solution, respectively. The pseudoequilibrium CO_2 uptakes of these three tests, defined as the CO_2 uptake when the outlet CO_2 concentration reached 95% of the inlet CO_2 concentration, are plotted in **Figure 6.** It is seen that the CO_2 uptake using ambient air lies between the CO_2 uptakes using simulated air of 0 and 85% RH. The CO_2 uptake at 0% RH is consistent with the CO_2 uptake

measured by the SAP instrument. This result shows that humidity has a significant impact on improving the CO_2 uptake due to the co-adsorption of H_2O, which enhances CO_2 adsorption onto supported amine sorbents. Another cause for the higher CO_2 uptake using ambient air is the higher CO_2 concentration in ambient air (400-500 ppm) than simulated air (400 ppm). However, as indicated by the SAP CO_2 adsorption experiments, increasing CO_2 concentration by this extent has a relatively small effect on increasing CO_2 uptake. It is therefore presumed that compared to the effect of humidity, the variation in indoor ambient CO_2 concentration plays a relatively minor role.

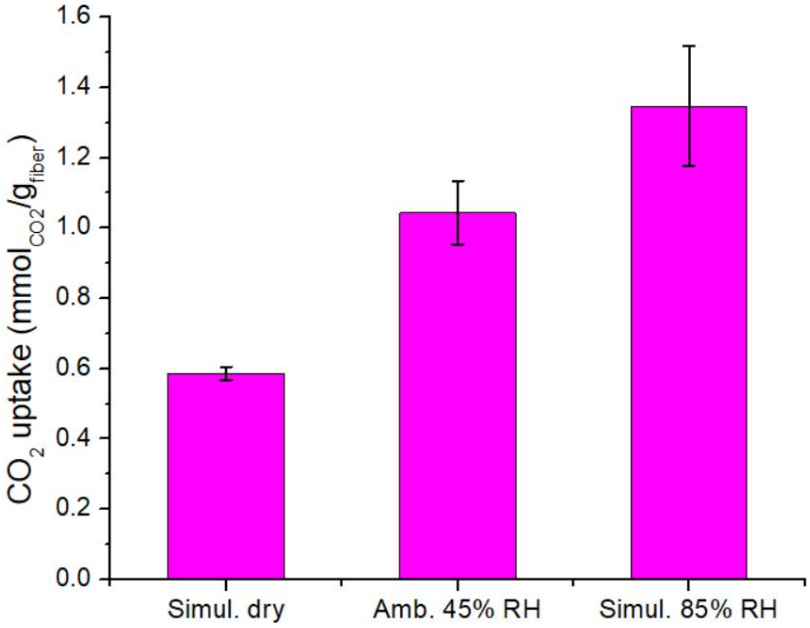

***Figure 6**. Comparison of the pseudoequilibrium CO_2 uptakes using indoor air and simulated air. CO_2 concentration = 450 ± 50 ppm, T = 22 °C ± 2 °C, RH = 45 ± 5%.*

3.3. Comparing the Kinetics of Fibers Impregnated in PEI Solutions of Different Concentrations

Breakthrough experiments were conducted using ambient air with 0.37PEI@SiO_2 and 1.04PEI@SiO_2 fibers to study the influence of PEI loading on adsorption kinetics using an inlet air velocity of 0.57 m/s. The breakthrough curves are shown in **Figure 7** (a). The integrated CO_2 uptake curves are shown in **Figure 7** (b). The integrated CO_2 uptake is defined as the accumulated CO_2 adsorption onto the fibers at a given moment. As the plot indicates, the

0.37PEI@SiO_2 fibers show an S-shaped breakthrough curve while the 1.04PEI@SiO_2 fibers show an immediate breakthrough at the beginning of the adsorption phase. The integrated CO_2 uptake curves also demonstrate a clear contrast between the two types of fibers. The 0.37PEI@SiO_2 fibers show a much greater slope and reach an elevated CO_2 (0.68 mmol/g) uptake much earlier (3000 s), as compared to the moderately higher CO_2 uptake (0.95 mmol/g) achieved in much longer time (6000 s) by the 1.04PEI@SiO_2 fibers. This suggests that the 0.37PEI@SiO_2 fibers have a significantly faster rate of mass transfer, likely due to differences in the extent of PEI pore blockage in the two samples. As shown in Table 1, the BET surface area of 0.37PEI@SiO_2 is four times greater than that of the 1.04PEI@SiO_2 fibers, and the pore volume of the 0.37PEI@SiO_2 fibers is five times greater than that of the 1.04PEI@SiO_2 fibers. The 0.37PEI@SiO_2 material has considerably greater contact area between CO_2 and PEI than the 1.04PEI@SiO_2 fibers, where PEI has likely blocked the pores and formed a layer on the surface of the fibers, making it difficult for CO_2 to access sorption sites. On the other hand, the CO_2 capacity of the 0.37PEI@SiO_2 fibers is 30% lower than that of the 1.04PEI@SiO_2 fibers. Considering that superior kinetics often outweighs the importance of a moderately higher CO_2 capacity, we elected to perform the following breakthrough studies using the 0.37PEI@SiO_2 fibers.

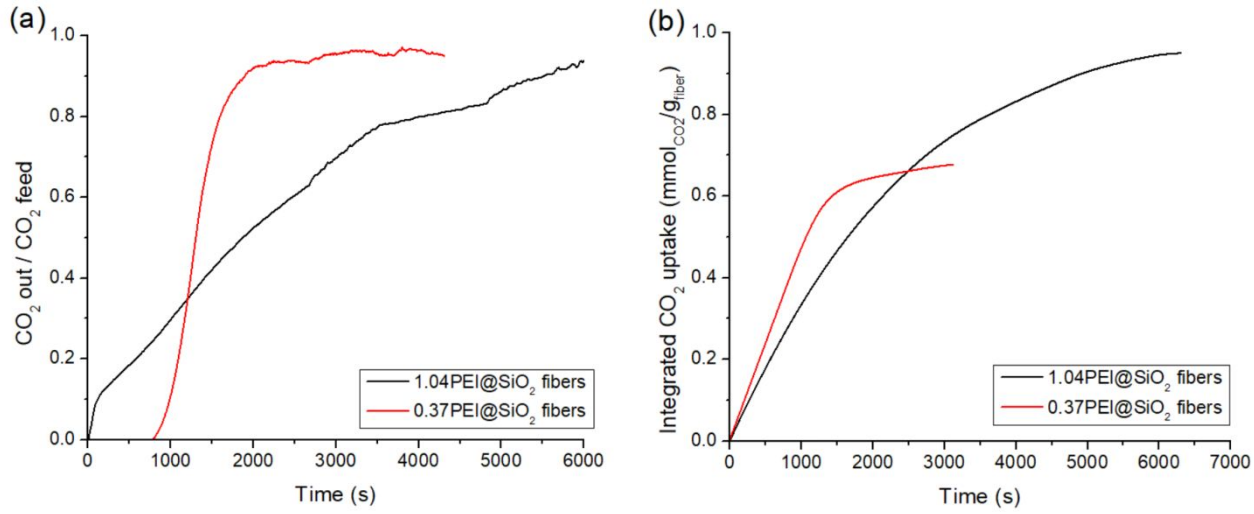

***Figure 7**. (a) breakthrough curves and (b) integrated CO_2 uptake curves on 0.37PEI@SiO_2 and 1.04PEI@SiO_2 fibers using ambient air at 0.57 m/s. CO_2 concentration = 450 ± 50 ppm, T = 22 °C ± 2 °C, RH = 45 ± 5%.*

3.4. Fiber Durability

Ambient air was used to test the breakthrough behavior of the 0.37PEI@SiO_2 fibers over multiple cycles. In total, 12 adsorption-desorption consecutive cycles were performed with a relative humidity of 45 ± 5%. The inlet air flow rate was varied between 0.17 to 1.1 m/s in these tests. Tests 1, 3, 5, 8 and 12 were conducted at identical conditions with an inlet air velocity of 0.57 m/s to observe if any loss in capacity occurred throughout the tests. The other tests used different inlet air velocities to study the effects of gas velocity on the kinetic performance of the fibers, as discussed in the following sections. The pseudoequilibrium capacities of these five cycles are shown in **Figure 8**.

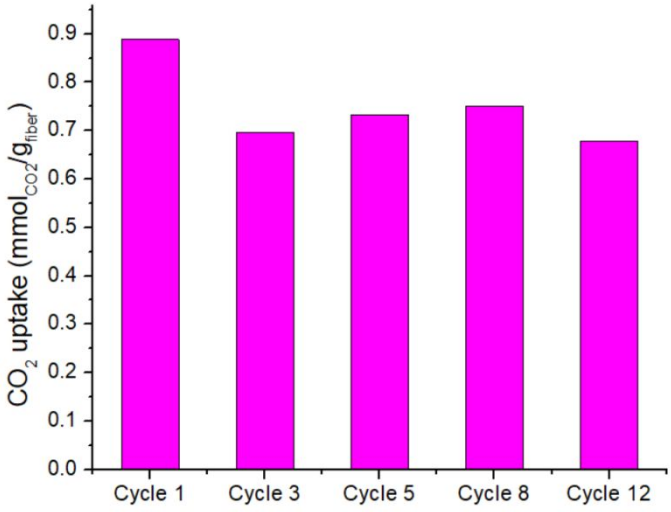

Figure 8. *Pseudoequilibrium CO_2 capacities of cycles 1, 3, 5, 8 and 12 conducted at 0.57 m/s air velocity. CO_2 concentration = 450 ± 50 ppm, T = 22 °C ± 2 °C, RH = 45 ± 5%.*

Figure 8 shows that the CO_2 capacity did not deteriorate significantly throughout the 12 cycles. The largest capacity loss occurred after cycle 1, where the capacity decreased by 22% from cycle 1 to cycle 3. Afterward, the CO_2 capacity stayed relatively stable. From cycle 3 to cycle 12, the CO_2 capacity only decreased by 3%.

The water content adsorbed by the fibers was also measured by the Li-Cor detector. The amount of water adsorbed at the pseudoequilibrium capacity is ~6 mmol/g fiber.

3.5. Influence of Varying Inlet Air Velocities

Inlet air velocity is an important parameter for practical deployment of DAC, since cycle times should be short and the feed is highly dilute. Higher air velocity leads to faster mass transfer (reduced external mass transfer resistance) and hence more favorable CO_2 adsorption kinetics, but also entails higher energy consumption by the fans that provide air movement. In this work, air velocity was varied between 0.17 to 1.1 m/s to explore its influence on CO_2 breakthrough performance. **Figure 9** (a) shows the breakthrough curves of cycles 4, 5, 6, and 10, where the inlet air velocities were 0.17, 0.57, 0.35, and 1.1 m/s, respectively (note that the air velocities of cycles 5 and 6 are not in ascending order, as the other cycles are). These air velocities correspond to a contact time between air and fibers of 0.59, 0.18, 0.29, and 0.09 s, respectively. To compare the shapes of these curves on a normalized basis, **Figure 9** (b) was plotted, where the x axis is normalized as the stoichiometric breakthrough time by multiplying the breakthrough time by the inlet air velocity. At the same x value, an equal amount of air will have passed through the reactor regardless of the air velocity. The plot indicates that the curves of cycles 4, 5, and 6 have similar shapes, where the CO_2 breakthrough occurs at the same CO_2 loading. For cycle 10, however, the breakthrough occurs at a lower CO_2 loading. This suggests that air velocity does not have significant influences on the breakthrough behavior when it is in the range of 0.17 to 0.57 m/s. This regime is suggestive of external mass transfer limitation. However, when air velocity is increased to 1.1 m/s, the breakthrough curve broadens as the breakthrough capacity decreases, which is a classic fingerprint of internal mass transfer limitations. It is noted that this reduction in the breakthrough capacity does not necessarily mean a decline in the overall performance using this high inlet air velocity, because in industrial DAC operations the optimal point to end the adsorption phase is usually well after the point of breakthrough to maximize the CO_2 productivity instead of the CO_2 uptake.

During the experiments, the pressure drop along the sorbent bed was less than 70 Pa across the range of inlet air velocities tested. At industrial scale, the pressure drop in the DAC system is not expected to vary significantly from this value, though ΔP will continue to increase as gas velocity increases. This suggests that the pressure drop will not be an obstacle to the implementation of the proposed fiber-based DAC system at larger scales.

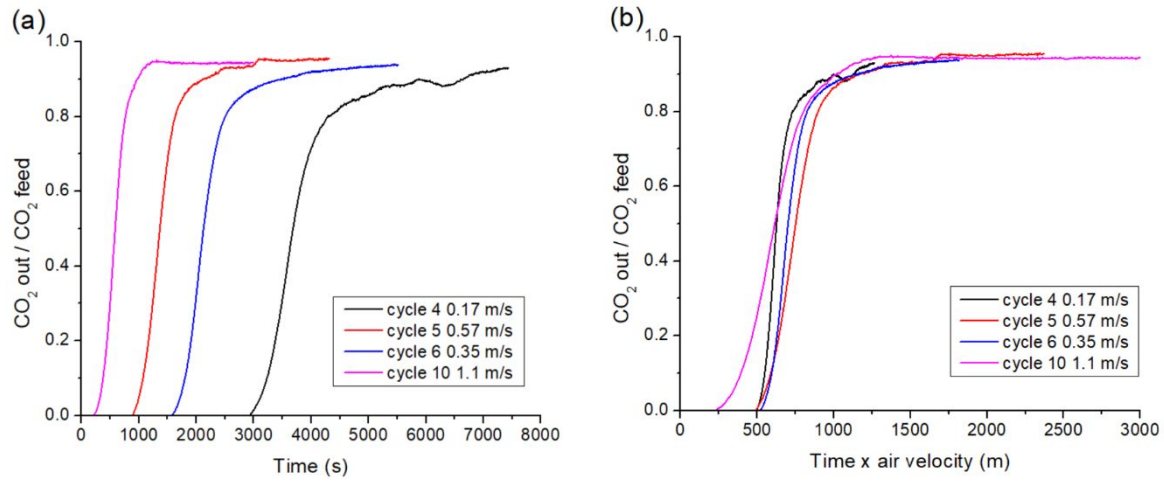

***Figure 9**. (a) Breakthrough curves and (b) normalized breakthrough curves for cycles 4, 5, 6 and 10 with varying air velocities. CO_2 concentration = 450 ± 50 ppm, T = 22 °C ± 2 °C, RH = 45 ± 5%.*

3.6. Optimizing Productivity

The performance of practical DAC systems depends more on the CO_2 productivity, i.e., the amount of CO_2 adsorbed per unit amount of fiber per unit time, as shown in Equation 3, than on other commonly measured parameters like the breakthrough capacity.[45,46,70] The productivity is influenced by the shape of the breakthrough curve, the time of the adsorption phase, and the time of desorption phase and other procedures of the cycle, such as cooling. The productivity as a function of the inlet air velocity and the duration of the adsorption phase is plotted in **Figure 10** (a), where the duration of the rest of the cycle (desorption phase, cooling phase, etc.) is assumed to be 15 minutes in this work. This estimate for the desorption time is chosen to be representative of technically achievable desorption times using current materials and systems. The sensitivity of the productivity estimates to the desorption times are shown in **Figure 11**, where the productivity was calculated by assuming the desorption time to be 3, 30, and 60 min, respectively.

$$\text{productivity} = \frac{\text{CO}_2\text{ uptake (mmol)}}{\text{wt of fibers (g)} \times (\text{adsorption (h)} + \text{desorption and other phases of the cycle (h)})} \quad (3)$$

As shown in **Figure 10**, for each inlet air velocity, there exists an optimal duration of the adsorption phase that gives the maximum productivity achievable using this air velocity. The maximum productivity achieved in these tests is 1.2 mmol of CO_2 per gram of fiber per hour, and it is

achieved using an inlet air velocity of 1.1 m/s and an adsorption time of 11 min. Note that this productivity assumes nearly total recovery of CO_2 from the desorption phase, because in these experiments, each adsorption phase was preceded by a desorption phase of 10 min under N_2 flow at 110 °C. In the industrial setup, the CO_2 recovery from the desorption phase may not be as complete as in these tests, resulting in a lower swing capacity, and hence the productivities can potentially be lower.

Figure 10 (b) plots the maximum productivity that can be achieved at each inlet air velocity. As the inlet air velocity increases, the maximum achievable productivity also increases. The shape of the graph indicates that the productivity has not yet reached a plateau at an inlet air velocity of 1.1 m/s, suggesting that further increasing the inlet air velocity should lead to higher productivities. Studies using higher inlet air velocities should be conducted in the future, as higher values could not be achieved with the current experimental set-up.

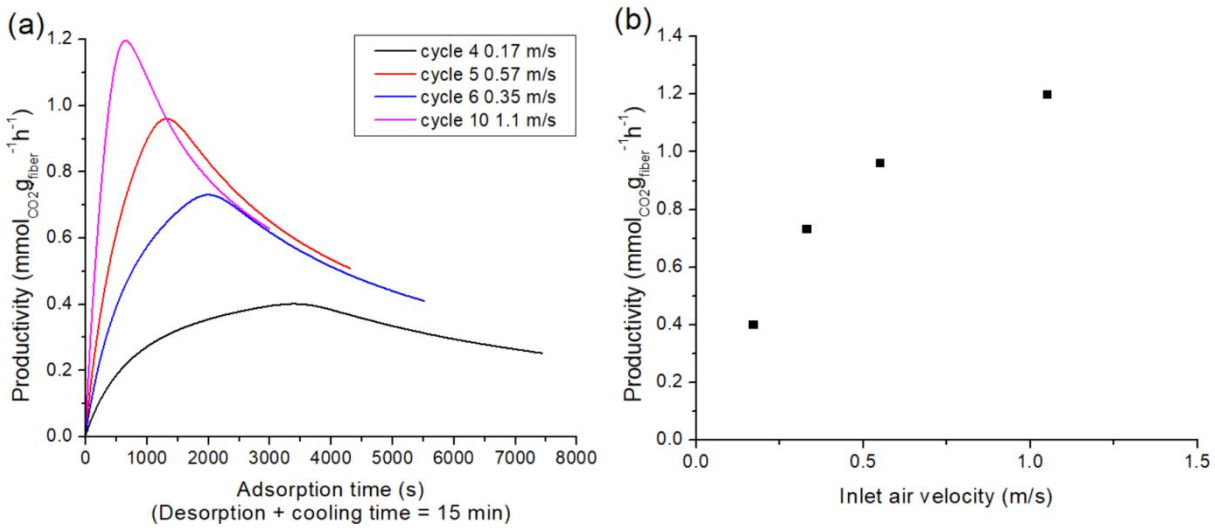

***Figure 10**. (a) Productivity as a function of the duration of adsorption phase and inlet air velocity (b) maximum productivity achievable at varying inlet air velocities. CO_2 concentration = 450 ± 50 ppm, T = 22 °C ± 2 °C, RH = 45 ± 5%.*

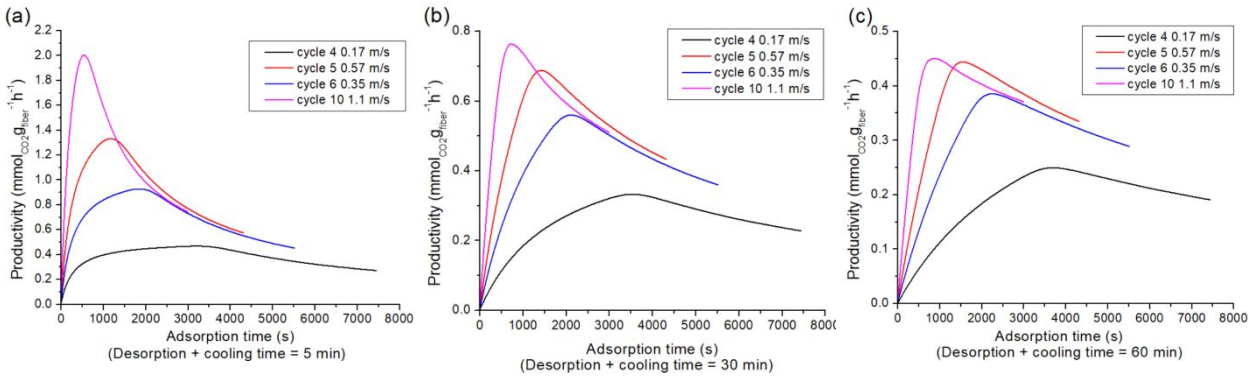

Figure 11. *Productivity as a function of duration of adsorption phase and inlet air velocity with a desorption phase duration of (a) 5 min (b) 30 min (c) 60 min. CO_2 concentration = 450 ± 50 ppm, T = 22 °C ± 2 °C, RH = 45 ± 5%.*

3.7. Kinetic Study of Steam Desorption

Steam desorption dynamics were studied using indirect contact heating to verify that the desorption phase is reasonably fast and that the assumption of a 15-minute desorption phase used above is valid. The steam desorption study conducted in this work is based on indirect contact heating, which differs from direct contact heating used in some industrial operations. However, it can be assumed that direct contact heating will lead to equivalent or faster desorption kinetics than indirect contact heating because of lower heat transfer resistance.

In this experiment, 0.3 g of 1.04PEI@SiO_2 fibers first underwent an adsorption phase using ambient air at a velocity of 0.57 m/s to reach their pseudoequilibrium capacity. After the adsorption, steam was passed through the heating jacket to indirectly exchange heat with the sample module. Steam flowed through the shell side of the reactor module, where heat was transferred to the stainless-steel reactor module and the fibers inside the module. Condensation was observed outside the sample module during the steam contact and the temperature of the sample module was measured to be constantly 100 °C during the desorption, meaning that the steam exchanging heat with the sample module was mostly saturated steam instead of highly superheated steam. After the desorption, another adsorption-desorption cycle was performed after the fibers had cooled. The CO_2 desorption curves and the accumulated CO_2 desorption from the two cycles are shown in **Figure 12** a and b, respectively. As shown in the plots, the rate of CO_2 desorption

increased rapidly during the first 30 s of the desorption. The rate of CO_2 desorption reached a maximum rapidly and then gradually decreased. After the initial 5 min, the outlet CO_2 concentration became negligible.

Figure 12 c shows the CO_2 uptakes during the two adsorption phases and the amounts of CO_2 desorbed during the first 5 min of the two desorption phases. The plot suggests that in the first cycle, 95% of the captured CO_2 was released within the first 5 min of the desorption phase. In the second cycle, this ratio became 98%. Compared to the experiments discussed earlier in this paper, where desorption was carried out for long periods using heating tape at 110 °C, using steam as the desorption agent results in a lower CO_2 swing capacity, but the difference is not significant. It has been shown by this set of experiments that the swing capacity obtained using steam is at least 95% of that using heating tapes. Assuming a desorption phase of 5 min followed by a cooling phase of 5 min with a swing capacity that is 95% of the maximum capacity, we can achieve a maximum productivity of 1.42 mmol of CO_2 per gram of fiber per hour. This validates the assumption of a 15-min desorption and cooling time used in the productivity calculation in the previous section.

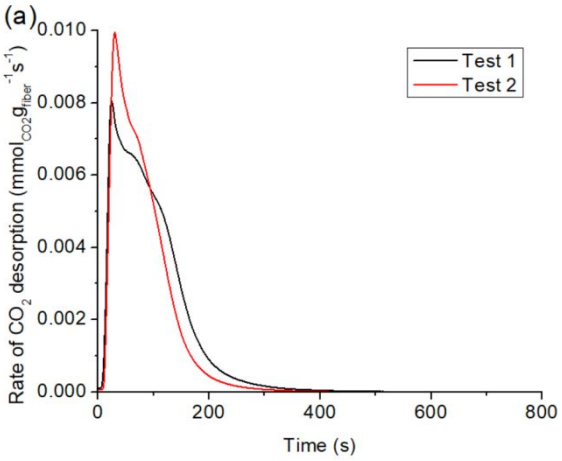

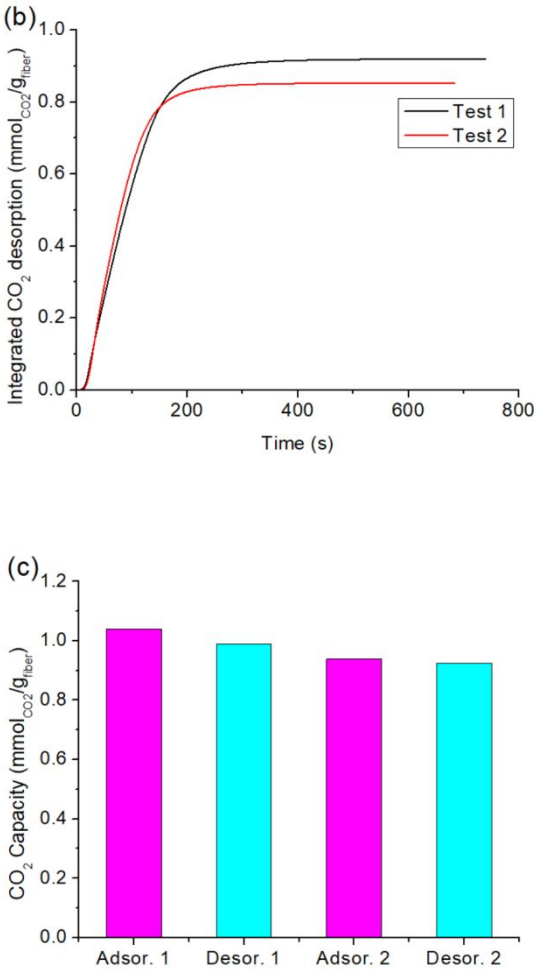

***Figure 12**. (a) Rate of CO_2 desorption (b) integrated CO_2 desorption curves for two consecutive tests using 100 °C steam. The fibers first underwent an adsorption phase using ambient air at a velocity of 0.57 m/s to reach the pseudoequilibrium capacity (CO_2 concentration = 450 ± 50 ppm, T = 22 °C ± 2 °C, RH = 45 ± 5%). (c) CO_2 uptakes reached in the two adsorption phases and the amounts of CO_2 desorbed in the first 5 min of the two desorption phases. Note: columns 2 and 4 depict the amount of CO_2 desorbed from the desorption phase, not the amount of CO_2 remaining on the fibers.*

4. Conclusions

This work investigated the dynamics of adsorption and desorption of fiber DAC sorbents in a fixed bed reactor. Fibers containing 52 wt% silica and 48% CA were spun and impregnated with PEI of different loadings. The fibers were characterized by SEM, N_2 physisorption, CO_2 isotherms, and

TGA combustion. The dynamic behavior of CO_2 adsorption was studied in a custom-built fixed fiber contactor where simulated air, both dry and humid, and ambient indoor air were used for breakthrough studies. The desorption of CO_2 by indirect heating with steam was studied by flowing steam to the shell side of the fixed bed.

The results show that ambient air and dry simulated air can have considerably different CO_2 capacities. Due to the ~50% relative humidity present in ambient air, the pseudoequilibrium capacities using ambient air were ~80% greater than dry, simulated air. Although fibers impregnated in 10% PEI solution had a lower PEI loading than fibers impregnated in 20% PEI solution (0.37 g PEI/g silica as compared to 1.04 g PEI/g sillica), leading to a lower pseudoequilibrium capacity (0.68 mmol/g as compared to 0.95 mmol/g), they had superior kinetics in CO_2 breakthrough experiments. The 0.37PEI@SiO_2 fibers demonstrated good stability over 12 adsorption-desorption cycles. The CO_2 breakthrough curves only changed shape when the inlet air velocity was increased from 0.57 to 1.1 m/s, indicating the onset of controlling internal mass transfer resistances. The maximum CO_2 productivity achieved so far, assuming a desorption phase of 15 min, is 1.2 mmol/g/h. This was achieved by using an inlet air velocity of 1.1 m/s on 0.37PEI@SiO_2 fibers. Desorption by indirect contact with steam showed promising kinetic behavior. The CO_2 outlet concentration reached the maximum rapidly in the first 30 s and >95% adsorbed CO_2 could be desorbed in the first 5 min of steam contact.

The key limitations of this study include the following. First, the inlet air velocities used in these experiments were still 3-10x lower than what would be expected for industrial operations. The key observations of this study, i.e. that a lower amine loading leads to better adsorption kinetics, and that the humidity in the air leads to better overall performance, may change when the air velocity is further increased. Second, only two PEI loadings were tested in detail, and it would be beneficial to test other loadings in the future to identify a potential optimum. Third, the tests were conducted at a relatively small scale using a sample tube with an inner diameter of 0.43 cm with 0.3 g fibers. Once the system is scaled up, the trends observed for adsorption and desorption dynamics may change. Therefore, experiments in larger sample tubes containing a larger quantity of fibers are recommended.

Author contributions'

Fanhe Kong: conceptualization, data curation, formal analysis, investigation, methodology, validation, visualization, writing (original & revisions)
Guanhe Rim: investigation, validation

Pranjali Priyadarshini: investigation, validation
MinGyu Song: investigation, validation
Matthew J. Realff: conceptualization, funding acquisition, methodology, project administration, resources, supervision,
Ryan P. Lively: conceptualization, funding acquisition, methodology, project administration, resources, supervision, writing (review & editing)
Christopher W. Jones: conceptualization, funding acquisition, methodology, project administration, resources, supervision, writing (review & editing)

Conflicts of Interest

The authors declare the following competing financial interest(s): C.W.J. has a financial interest in Global Thermostat, which seeks to commercialize CO_2 capture from air. This work is not affiliated with Global Thermostat. C.W.J. has a conflict-of-interest management plan in place at Georgia Tech.

Acknowledgements

The authors thank the Georgia Tech Direct Air Capture Center, DirACC, for fruitful discussions. The information, data, or work presented herein was funded in part by the Advanced Research Projects Agency-Energy (ARPA-E), U.S. Department of Energy, under Award Number DE-AR0001309. The views and opinions of authors expressed herein do not necessarily state or reflect those of the United States Government or any agency thereof.

References

1. Lackner, K. S. Capture of carbon dioxide from ambient air. *Eur. Phys. J. Spec. Top.* **176**, 93–106 (2009).
2. Breyer, C., Fasihi, M., Bajamundi, C. & Creutzig, F. Direct Air Capture of CO_2: A Key Technology for Ambitious Climate Change Mitigation. *Joule* **3**, 2053–2057 (2019).
3. Beuttler, C., Charles, L. & Wurzbacher, J. The Role of Direct Air Capture in Mitigation of Anthropogenic Greenhouse Gas Emissions. *Front. Clim.* **1**, 10 (2019).
4. McQueen, N., Gomes, K.V., McCormick, C., Blumanthal, K., Pisciotta, M. & Wilcox, J. A. review of direct air capture (DAC): scaling up commercial technologies and innovating for the future. *Prog. Energy* **3**, 032001 (2021).

5. Jacobson, M. Z. The health and climate impacts of carbon capture and direct air capture. *Energy Environ. Sci.* **12**, 3567–3574 (2019).
6. Lackner, K. S. & Azarabadi, H. Buying down the Cost of Direct Air Capture. *Ind. Eng. Chem. Res.* **60**, 8196–8208 (2021).
7. Azarabadi, H. & Lackner, K. S. Postcombustion Capture or Direct Air Capture in Decarbonizing US Natural Gas Power? *Environ. Sci. Technol.* **54**, 5102–5111 (2020).
8. Sutherland, B. R. Pricing CO_2 Direct Air Capture. *Joule* **3**, 1571–1573 (2019).
9. Holmes, H. E., Lively, R. P. & Realff, M. J. Defining Targets for Adsorbent Material Performance to Enable Viable BECCS Processes. *JACS Au* **1**, 795–806 (2021).
10. Stavrakas, V., Spyridaki, N. A. & Flamos, A. Striving towards the deployment of bio-energy with carbon capture and storage (BECCS): A review of research priorities and assessment needs. *Sustain.* **10**, 2206 (2018).
11. Gambhir, A. & Tavoni, M. Direct Air Carbon Capture and Sequestration: How It Works and How It Could Contribute to Climate-Change Mitigation. *One Earth* **1**, 405–409 (2019).
12. Haertel, C.J.J., McNutt, M., Ozkan, M., Aradóttir, E.S., Valsaraj, K.T., Sanberg, P.R., Talati, S. & Wilcox, J. The promise of scalable direct air capture. *Chem* **7**, 2831–2834 (2021).
13. Marcucci, A., Kypreos, S. & Panos, E. The road to achieving the long-term Paris targets: energy transition and the role of direct air capture. *Clim. Change* **144**, 181–193 (2017).
14. de Jonge, M. M. J., Daemen, J., Loriaux, J. M., Steinmann, Z. J. N. & Huijbregts, M. A. J. Life cycle carbon efficiency of Direct Air Capture systems with strong hydroxide sorbents. *Int. J. Greenh. Gas Control* **80**, 25–31 (2019).
15. Kong, F., Rim, G., Song, M., Rosu, C., Priyadarshini, P., Lively, R. P., Realff, M. J. & Jones, C. W. Research needs targeting direct air capture of carbon dioxide: Material & process performance characteristics under realistic environmental conditions. *Korean J. Chem. Eng.* **39**, 1-19 (2022).
16. Sanz-Pérez, E. S., Murdock, C. R., Didas, S. A. & Jones, C. W. Direct Capture of CO_2 from Ambient Air. *Chem. Rev.* **116**, 11840–11876 (2016).
17. Zhu, X., Xie, W., Wu, J., Miao, Y., Xiang, C., Chen, C., Ge, B., Gan, Z., Yang, F., Zhang, M. & O'Hare, D. Recent advances in direct air capture by adsorption. *Chem. Soc. Rev.* **51**, 6574–6651 (2022).

18. Wilson, S. M. W. & Tezel, F. H. Direct Dry Air Capture of CO_2 Using VTSA with Faujasite Zeolites. *Ind. Eng. Chem. Res.* **59**, 8783–8794 (2020).
19. Wilson, S. M. W., Gabriel, V. A. & Tezel, F. H. Adsorption of components from air on silica aerogels. *Microporous Mesoporous Mater.* **305**, 110297 (2020).
20. Zhao, H.X., Li, J.C., Wang, Y., Guo, Y.R., Li, S. & Pan, Q.J. An environment-friendly technique for direct air capture of carbon dioxide via a designed cellulose and calcium system. *Sep. Purif. Technol.* **307**, 122774 (2023).
21. Sehaqui, H., Gálvez, M.E., Becatinni, V., Cheng Ng, Y., Steinfeld, A., Zimmermann, T. & Tingaut, P. Fast and reversible direct CO_2 capture from air onto all-polymer nanofibrillated cellulose-polyethylenimine foams. *Environ. Sci. Technol.* **49**, 3167–3174 (2015).
22. McQueen, N., Kelemen, P., Dipple, G., Renforth, P. & Wilcox, J. Ambient weathering of magnesium oxide for CO_2 removal from air. *Nat. Commun.* **11**, 3299 (2020).
23. Zhu, X., Ge, T., Yang, F., Lyu, M., Chen, C., O'Hare, D. & Wang, R. Efficient CO_2 capture from ambient air with amine-functionalized Mg-Al mixed metal oxides. *J. Mater. Chem. A* **8**, 16421–16428 (2020).
24. Fujikawa, S., Selyanchyn, R. & Kunitake, T. A new strategy for membrane-based direct air capture. *Polym. J.* **53**, 111-119 (2021).
25. Zeman, F. Reducing the cost of ca-based direct air capture of CO_2. *Environ. Sci. Technol.* **48**, 11730–11735 (2014).
26. Wilson, S. M. W. High Purity CO_2 from Direct Air Capture Using a Single Tvsa Cycle with Na-X Zeolites. *Sep. Purif. Tec*hnol. **29**, 121186 (2022).
27. Wu, X., Krishnamoorti, R. & Bollini, P. Technological Options for Direct Air Capture: A Comparative Process Engineering Review. *Annu. Rev. Chem. Biomol. Eng.* **13**, 279–300 (2022).
28. Li, K., Kress, J.D. & Mebane, D.S. The mechanism of CO_2 adsorption under dry and humid conditions in mesoporous silica-supported amine sorbents. *J. Phys. Chem.* **120**, 23683-23691 (2016).
29. Wijesiri, Romesh P., Gregory P. Knowles, Hasina Yeasmin, Andrew FA Hoadley, & Alan L. Chaffee. "Desorption process for capturing CO_2 from air with supported amine sorbent." *Ind. Eng. Chem.* **58**, 15606-15618 (2019).
30. Ocean Studies Board & National Academies of Sciences, Engineering, and Medicine. Negative emissions technologies and reliable sequestration: A research agenda. (2019).

31. Modayil Korah, M., Ly, S., Stangherlin Barbosa, T., Nile, R., Jin, K., Lackner, K.S. & Green, M.D. Electrospun Poly (vinyl alcohol)–l-Arginine Nanofiber Composites for Direct Air Capture of CO_2. *ACS ES&T Eng*. (2022) https://doi.org/10.1021/acsestengg.2c00307
32. Elfving, J., Kauppinen, J., Jegoroff, M., Ruuskanen, V., Järvinen, L. & Sainio, T. Experimental comparison of regeneration methods for CO_2 concentration from air using amine-based adsorbent. *Chem. Eng. J.* **404**, 126337 (2021).
33. Gebald, C., Wurzbacher, J. A., Tingaut, P. & Steinfeld, A. Stability of amine-functionalized cellulose during temperature-vacuum-swing cycling for CO2 capture from air. *Environ. Sci. Technol.* **47**, 10063–10070 (2013).
34. Didas, S. A., Kulkarni, A. R., Sholl, D. S. & Jones, C. W. Role of amine structure on carbon dioxide adsorption from ultradilute gas streams such as ambient air. *ChemSusChem* **5**, 2058–2064 (2012).
35. Sabatino, F., Grimm, A., Gallucci, F., van Sint Annaland, M., Kramer, G. J. & Gazzani, M. A comparative energy and costs assessment and optimization for direct air capture technologies. *Joule* **5**, 2047–2076 (2021).
36. Tanthana, J. & Chuang, S. S. C. In situ infrared study of the role of PEG in stabilizing silica-supported amines for CO_2 capture. *ChemSusChem* **3**, 957–964 (2010).
37. Sanz-Pérez, E. S. Olivares-Martín, M., Arencibia, A., Sanz, R., Calleja, G. & Maroto-Valer, M. M. CO_2 adsorption performance of amino-functionalized SBA-15 under post-combustion conditions. *Int. J. Greenh. Gas Control* **17**, 366–375 (2013).
38. Liu, Y. Lin, X., Wu, X., Liu, M., Shi, R. & Yu, X. Pentaethylenehexamine loaded SBA-16 for CO_2 capture from simulated flue gas. *Powder Technol.* **318**, 186–192 (2017).
39. Bollini, P., Didas, S. A. & Jones, C. W. Amine-oxide hybrid materials for acid gas separations. *J. Mater. Chem.* **21**, 15100–15120 (2011).
40. Didas, S. A., Choi, S., Chaikittisilp, W. & Jones, C. W. Amine-Oxide Hybrid Materials for CO_2 Capture from Ambient Air. *Acc. Chem. Res.* **48**, 2680–2687 (2015).
41. Serna-Guerrero, R., Da'na, E. & Sayari, A. New insights into the interactions of CO_2 with amine-functionalized silica. *Ind. Eng. Chem. Res.* **47**, 9406–9412 (2008).
42. Rim, G., Kong, F., Song, M., Rosu, C., Priyadarshini, P., Lively, R. P. & Jones, C. W. Sub-Ambient Temperature Direct Air Capture of CO_2 using Amine-Impregnated MIL-101 (Cr) Enables Ambient Temperature CO_2 Recovery. *JACS Au* **2**, 380-393 (2022).

43. Song, M., Rim, G., Kong, F., Priyadarshini, P., Rosu, C., Lively, R.P. & Jones, C.W. Cold-Temperature Capture of Carbon Dioxide with Water Coproduction from Air Using Commercial Zeolites. *Ind. Eng. Chem. Res.* **61**, 13624–13634 (2022).
44. Wilson, S. M. W. The potential of direct air capture using adsorbents in cold climates. Iscience **25**, 105564 (2022).
45. Sinha, A., Darunte, L. A., Jones, C. W., Realff, M. J. & Kawajiri, Y. Systems Design and Economic Analysis of Direct Air Capture of CO_2 through Temperature Vacuum Swing Adsorption Using MIL-101(Cr)-PEI-800 and mmen-Mg2(dobpdc) MOF Adsorbents. *Ind. Eng. Chem. Res.* **56**, 750–764 (2017).
46. Sinha, A., Darunte, L. A., Jones, C. W., Realff, M. J. & Kawajiri, Y. Correction to “Systems Design and Economic Analysis of Direct Air Capture of CO_2 through Temperature Vacuum Swing Adsorption Using MIL-101(Cr)-PEI-800 and mmen-Mg2(dobpdc) MOF Adsorbents”. *Ind. Eng. Chem. Res.* **59**, 503–505 (2020).
47. Eisaman, M. D. Negative Emissions Technologies: The Tradeoffs of Air-Capture Economics. *Joule* **4**, 516–520 (2020).
48. Azarabadi, H. & Lackner, K. S. A sorbent-focused techno-economic analysis of direct air capture. *Appl. Energy* **250**, 959–975 (2019).
49. Fasihi, M., Efimova, O. & Breyer, C. Techno-economic assessment of CO_2 direct air capture plants." J. Clean. Prod. **224**, 957-980 (2019).
50. Qiu, Y., Lamers, P., Daioglou, V., McQueen, N., de Boer, H.S., Harmsen, M., Wilcox, J., Bardow, A. & Suh, S. Environmental trade-offs of direct air capture technologies in climate change mitigation toward 2100. *Nat. Commun.* **13**, 3635 (2022).
51. Wurzbacher, J. A., Gebald, C., Brunner, S. & Steinfeld, A. Heat and mass transfer of temperature-vacuum swing desorption for CO_2 capture from air. *Chem. Eng. J.* **283**, 1329–1338 (2016).
52. Darunte, L. A., Terada, Y., Murdock, C. R., Walton, K. S., Sholl, D. S. & Jones, C. W. Monolith-Supported Amine-Functionalized Mg2(dobpdc) Adsorbents for CO_2 Capture. *ACS Appl. Mater. Interfaces* **9**, 17042–17050 (2017).
53. Sujan, A. R., Pang, S. H., Zhu, G., Jones, C. W. & Lively, R. P. Direct CO_2 capture from air using poly (ethylenimine)-loaded polymer/silica fiber sorbents." *ACS Sustain. Chem. Eng.* **7**, 5264-5273 (2019).

54. Wilfong, W. C., Wang, Q., Ji, T., Baker, J. S., Shi, F., Yi, S. & Gray, M. L. Directly Spun Epoxy-Crosslinked Polyethylenimine Fiber Sorbents for Direct Air Capture and Postcombustion Capture of CO_2. *Energy Technology* **10**, 2200356 (2022).

55. Deng, Y., Li, J., Miao, Y. & Izikowitz, D. A comparative review of performance of nanomaterials for Direct Air Capture. *Energy Reports* **7**, 3506–3516 (2021).

56. Grossmann, Q., Stampi-Bombelli, V. & Mazzotti, M. Molecular to process scale: A review of holistic direct air capture contactor design. *11th Trondheim Conf. CO_2 Capture, Transp. Storage* 450–454 (2021).

57. Lawson, S., Baamran, K., Newport, K., Rezaei, F. & Rownaghi, A. A. Formulation and processing of dual functional Adsorbent/Catalyst structured monoliths using an additively manufactured contactor for direct Capture/Conversion of CO_2 with cogeneration of ethylene. *Chem. Eng. J.* **431**, 133224 (2022).

58. Labreche, Y., Lively, R. P., Rezaei, F., Chen, G., Jones, C. W. & Koros, W. J. Post-spinning infusion of poly(ethyleneimine) into polymer/silica hollow fiber sorbents for carbon dioxide capture. *Chem. Eng. J.* **221**, 166–175 (2013).

59. Lively, R. P., Chance, R. R., Kelley, B. T., Deckman, H. W., Drese, J. H., Jones, C. W. & Koros, W. J. Hollow fiber adsorbents for CO_2 removal from flue gas. *Ind. Eng. Chem.* **48**, 7314-7 (2009).

60. Li, F. S., Qiu, W., Lively, R. P., Lee, J. S., Rownaghi, A. A. & Koros, W. J. Polyethyleneimine-functionalized polyamide imide (torlon) hollow-fiber sorbents for post-combustion CO_2 capture. *ChemSusChem* **6**, 1216–1223 (2013).

61. Quan, W., Holmes, H. E., Zhang, F., Hamlett, B. L., Finn, M. G., Abney, C. W., Kapelewski, M. T., Weston, S. C., Lively, R. P. & Koros, W. J. Scalable Formation of Diamine-Appended Metal-Organic Framework Hollow Fiber Sorbents for Postcombustion CO_2 Capture. *JACS Au* **2**, 1350-1358 (2022).

62. Chance, R., Chen, G., Dai, Y., Fan, Y., Jones, C., Kalyanaraman, J., Kawajiri, Y., Koros, W., Lively, R., McCool, B. & Pang, S., Rapid Temperature Swing Adsorption using Polymeric/Supported Amine Hollow Fibers. Georgia Institute of Technology, Atlanta, GA

63. Kalyanaraman, J., Fan, Y., Lively, R. P., Koros, W. J., Jones, C. W., Realff, M. J. & Kawajiri, Y. Modeling and experimental validation of carbon dioxide sorption on hollow

fibers loaded with silica-supported poly(ethylenimine). *Chem. Eng. J.* **259**, 737–751 (2015).

64. Labreche, Y., Fan, Y., Rezaei, F., Lively, R. P., Jones, C. W. and Koros, W. J. Poly(amide-imide)/silica supported PEI hollow fiber sorbents for postcombustion CO_2 capture by RTSA. *ACS Appl. Mater. Interfaces* **6**, 19336–19346 (2014).

65. Armstrong, M., Shi, X., Shan, B., Lackner, K. & Mu, B. Rapid CO_2 capture from ambient air by sorbent-containing porous electrospun fibers made with the solvothermal polymer additive removal technique. *AIChE J.* **65**, 214–220 (2019).

66. Sekizkardes, A. K., Kusuma, V. A., Culp, J. T., Muldoon, P., Hoffman, J., Steckel, J. A. & Hopkinson, D. Single polymer sorbent fibers for high performance and rapid direct air capture. J. Mater. Chem. (2023). DOI: https://doi.org/10.1039/D2TA09270K

67. Zhang, J., Zhao, Q., Wang, S. & Tan, X. Direct capture of low concentration CO_2 using tetraethylenepentamine-grafted polyacrylonitrile hollow fibers. *Sep. Purif. Technol.* **287**, 120562 (2022).

68. Lively, R. P., Leta, D. P., DeRites, B. A., Chance, R. R. & Koros, W. J. Hollow fiber adsorbents for CO_2 capture: Kinetic sorption performance. *Chem. Eng. J.* **171**, 801–810 (2011).

69. Rezaei, F., Lively, R. P., Labreche, Y., Chen, G., Fan, Y., Koros, W. J. and Jones, C. W. Aminosilane-grafted polymer/silica hollow fiber adsorbents for CO_2 capture from flue gas. *ACS Appl. Mater. Interfaces* **5**, 3921–3931 (2013).

70. Elfving, J., Bajamundi, C., Kauppinen, J. & Sainio, T. Modelling of equilibrium working capacity of PSA, TSA and TVSA processes for CO_2 adsorption under direct air capture conditions. *J. CO2 Util.* **22**, 270–277 (2017).